Global and Regional Moisture Analyses at NCEP

Russell E. Treadon, Hua-Lu Pan, Wan-Shu Wu, Ying Lin[1], William S. Olson[2], and Robert J. Kuligowski[3]

[1]*Environmental Modeling Center, NOAA/NWS/NCEP, Camp Springs, MD*
[2]*Joint Center for Earth Systems Technology, NASA/GSFC, Greenbelt, MD*
[3]*Office of Research and Applications, NOAA/NESDIS, Camp Springs, MD*

1. Introduction

While observing, analyzing, and forecasting changes in both global and regional distributions of moisture is one of the most important forecast elements in terms of socio-economic impact, it is also one of the most difficult aspects to consistently forecast with high skill. The reasons for this are many. Our understanding of the planet's water cycle remains incomplete both in terms of theory and modeling. Global observations of the pertinent processes remain incomplete. Even with currently available data, questions remain as to how best extract and integrate the information contained within the data with that which the models resolve and simulate.

This paper briefly reviews the current status of the analysis of moisture in the National Centers for Environmental Prediction (NCEP) global and regional data assimilation systems. Most of the following discussion pertains to the global system. Specific comments regarding the regional system are limited to the use of precipitation and cloud top pressure observations.

2. Changes to GFS moist physics

The prognostic variables in the NCEP global forecast system (GFS) model (formerly the medium range forecast (MRF) model) are spectral coefficients of specific humidity, virtual temperature, vorticity, divergence, and natural logarithm of the surface pressure. Cloud condensate was added as an additional history variable in May 2001. The equation governing the evolution of cloud condensate mixing ratio, q_c, is

$$\frac{\partial q_c}{\partial t} = -V \cdot \nabla q_c - \dot{\sigma} \frac{\partial q_c}{\partial \sigma} + S_c + S_g - P - E + F_{qc} \qquad (1)$$

The first two terms on the right hand side of (1) describe three-dimensional advection of q_c. The effects of convective and grid-scale condensation processes are represented by S_c and S_g, respectively. P and E are condensate sinks due to precipitation and evaporation. Finally, F_{qc} denotes the effects of horizontal and vertical diffusion. As formulated in the GFS, cloud condensate can be liquid water, mixed phase, or ice depending on the local temperature.

The GFS mass-flux cumulus parameterization, simplified Arakawa-Schubert or SAS, (Pan, 2000, *pers. comm.*) detrains condensate at the rate S_c from the convective cloud top. Prior to the May 2001 upgrade, the SAS cloud top was the level at which the parameterized convective parcel became neutrally buoyant with respect to its environment. Initial tests of the prognostic cloud condensate scheme indicated that tropical cloud top detrainment was unrealistically confined to just a few layers. In response to this, the SAS cloud top selection algorithm was changed. The convective cloud top is now randomly chosen to be a level between the level of neutral buoyancy and that of minimum moist static energy. The entrainment rate is then

re-computed to ensure that the parcel becomes neutrally buoyant at the selected cloud top. Unrelated to this change, but perhaps more important in terms of model performance was the inclusion of cumulus momentum mixing. The momentum exchange is calculated through the mass flux formulation in a manner similar to that for heat and moisture.

Grid-scale condensation, S_g, is based on Zhao and Carr (1997) with modifications taken from Sundqvist *et al.* (1989). Evaporation of cloud condensate is taken from Zhao and Carr (1997). The precipitation rate P for ice follows the parameterization of Zhao and Carr (1997), while that for the liquid phase follows Sundqvist *et al.* (1989). Subsequent to the May 2001 implementation, excessive amounts of light precipitation were noted. This was addressed through a minor implementation in August 2001. The autoconversion rate of ice was slightly modified along with an empirically based calculation of the effective radius for ice crystals (Hemysfield and McFarquhar, 1996).

The introduction of prognostic cloud condensate necessitated changes to the interaction of radiation and clouds. Fractional cloud cover, C, is diagnosed on each layer using the formula of Xu and Randall (1996),

$$C = \max\left[R^{0.25} \left(1 - \exp\left\{ - \frac{2000 \times \left(q_c - q_{cmin} \right)}{\min\left[\max\left(\left[\left(1 - R \right) \times q^* \right]^{0.25}, 0.0001 \right), 1.0 \right]} \right\}, 0.0 \right) \right] \tag{2}$$

where, R is the relative humidity, q^* is the saturation specific humidity, and q_{cmin} is a specified lower limit. Saturation specific humidity is computed with respect to water or ice surfaces in accordance with the temperature. Random overlap is assumed for clouds in all layers.

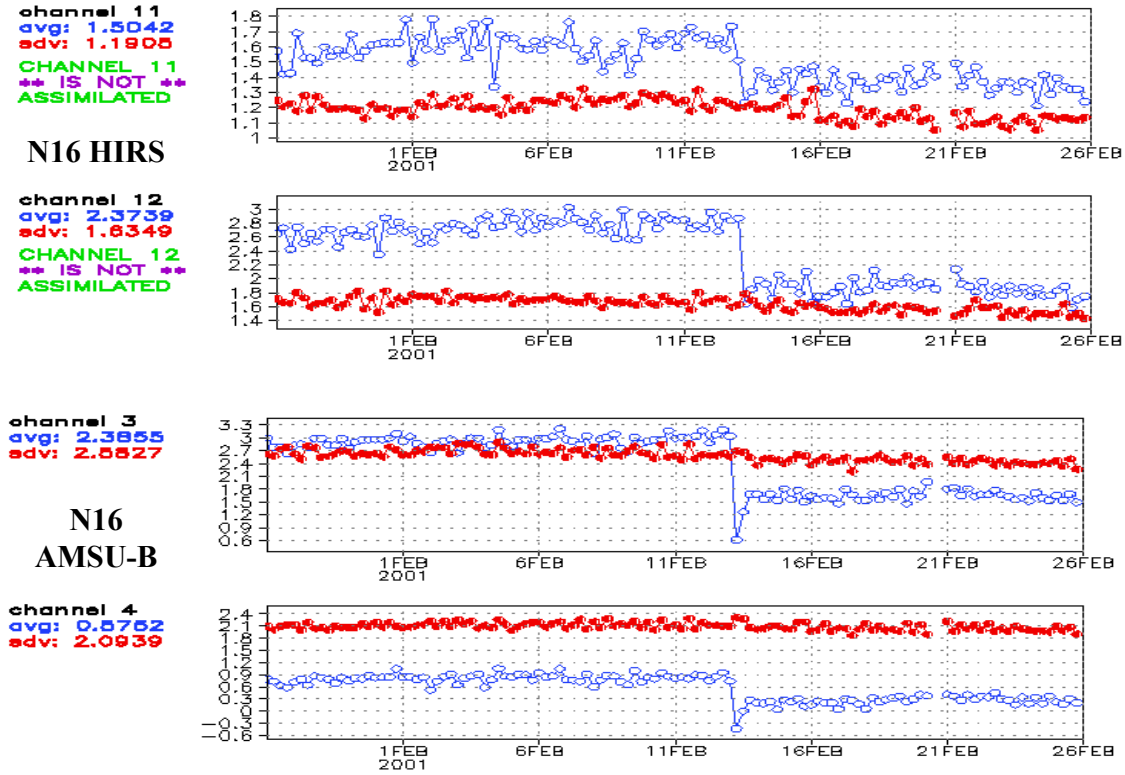

Figure 1 Time series of the average (blue) and standard deviation (red) of the global innovation for the indicated channels and instruments on NOAA-16.

Changes have been made to both the short- and long-wave radiation to make better use of the additional information that prognostic cloud condensate brings into the model. For shortwave radiation, the cloud optical thickness depends on the extinction coefficient and cloud condensate path. The extinction coefficient is parameterized as a linear function of the effective radius, which in turn is a function of cloud condensate. These changes follow the work of Slingo (1989), Chou *et al.* (1998), and Kiehl *et al.* (1998). Changes in the infrared portion of the spectrum follow the approach of the NCAR CCM (Stephens, 1984) in which cloud emissivity is calculated from the predicted cloud condensate.

An immediate benefit of the more complete and realistic representation of moisture is an improved fit of the GFS background to the mid- and upper-tropospheric moisture channels of HIRS and AMSU-B. This is seen in Fig. 1 which plots time series of the average and standard deviation of the global innovation for NOAA-16 HIRS/3 channels 11 and 12 and AMSU-B channels 4 and 5. The dramatic drop in the average innovation on 13 February coincides with placement of the prognostic cloud condensate model into EMC's (Environmental Modeling Center) parallel (pre-implementation) slot.

3. Observations

The global data assimilation system (GDAS) makes use of moisture observations from both conventional and satellite platforms. Conventional data include rawinsondes, marine buoys, and dropsondes (when available). Satellite radiances from GOES and HIRS sounders and AMSU radiometers provide moisture information. Additionally, the GDAS makes use of instantaneous rain rates derived from SSM/I and TRMM TMI brightness temperatures. The eta (regional) data assimilation system (EDAS) uses the above observations as available over its North American domain plus total column water vapor (TCWV) from GOES (over land) and SSM/I (over water). The SSM/I comes from the environmental data records of the operational FNMOC data stream. Rather than examine the impact of the above data sets, the discussion here focuses on microwave derived precipitation rates and the use of TCWV in the GDAS.

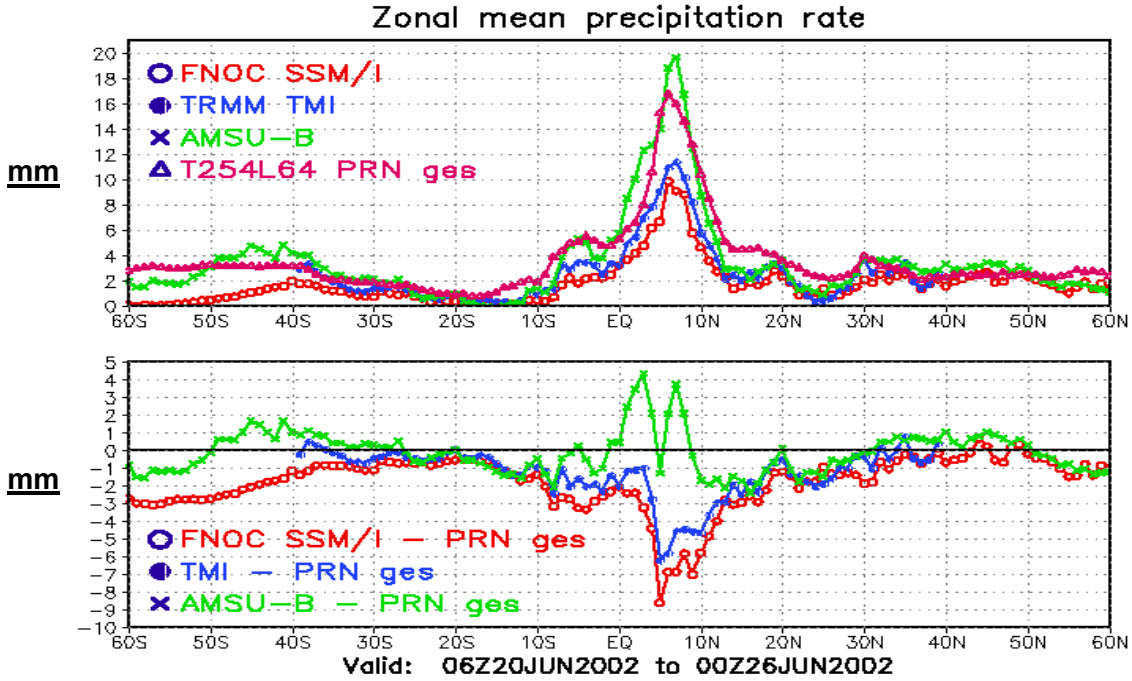

Figure 2 Zonal mean rain rates (upper panel) from three microwave-based algorithms (SSM/I, TMI, AMSU-B) and a pre-implementation T254L64 version of the GFS. Lower panel is the difference between the estimates and the GFS background. (PRN ges ≡ GFS background)

Instantaneous rain rates from the "Day-2" AMSU-B algorithm (Weng and Grody, 2000; Zhao and Weng, 2002) have been recently compared to rain rates from SSM/I (FNMOC operational algorithm, Ferraro, 1997) and TMI (2A-12 product, version 5, Kummerrow *et al.*, 2001). An initial comparison of the products with respect to the GFS background reveals two features (Fig. 2). First, GFS rain rates in the tropics are consistently higher than those derived from TMI and SSM/I. This is due to persistent areas of precipitation in the GFS background (e.g., Maritime and TMI. With respect to AMSU-B rain rates, however, the tropical GFS rain rates are, if anything, a bit too low. The AMSU-B rain rates are significantly higher than those derived from SSM/I and TMI. Moving out of the deep tropics, the algorithms and model yield comparable rates. Differences between the retrieved rain rates raise the question as to which product best represents the "truth." Definitively answering this question is difficult given the highly variable nature of precipitation and the lack of global, high quality "ground truth."

The degree of variation between the algorithms also raises issues of product suitability for assimilation purposes. AMSU-B rain rates possess a different bias, at least in terms of zonal means, from SSM/I and TMI products. The bias and error structures, in fact, are likely to be more complex. Given such variability and complexity, it is natural to consider whether direct radiance assimilation might be a more robust approach. Forward modeling of radiances in cloudy and precipitating fields of view presents it's own unique challenges. Still, the investment of time necessary to address and resolve these difficulties might allow for more effective and comprehensive use of radiances.

Past attempts to assimilate SSM/I TCWV (operational FNMOC algorithm, Alihouse et al., 1990; Colton and Poe, 1994) in the GDAS proved unsuccessful. SSM/I TCWV moistened the tropics while drying the extratropics. The tropical moistening occurred primarily in the lower troposphere. This increased the boundary layer convective available potential energy, which in turn, led to more vigorous convection in the GFS. The anomalous forcing associated with the more intense convection disrupted the Walker and eventually the Hadley circulations. Given that SSM/I TCWV compares well with validation datasets (Ferraro, pers. comm.), efforts were made to modify the GFS cumulus parameterization to maintain higher tropical TCWV values. Through experimentation it was found that changing a single parameter largely achieved this result. The parameter in question represents the percentage of falling convective precipitation that is available for evaporation. This parameter was increased from 7% to 30%. SSM/I assimilation tests following this modification yielded very positive results. Neither the Walker nor Hadley circulations were adversely affected. Precipitation skill scores over the continental U.S. improved, most significantly being a reduction in the bias. Improvements were also noted in the skill of tropical cyclone tracks over the Atlantic and Eastern Pacific basins.

In light of this positive impact, SSM/I assimilation was slated for further parallel testing. While awaiting this test, TCWV retrieved from AMSU-A radiances (Grody et al., 2001) became available and was compared with that from SSM/I and GFS. Quite surprisingly the difference between the AMSU-A and GFS TCWV was significantly smaller than that between the GFS and SSM/I (Fig. 3). Not only is the difference smaller, but it also has the opposite sign (in terms of zonal means). Similar to the SSM/I product, the AMSU-A TCWV product has been validated against ground "truth." How, then, can the differences be reconciled?

The difference in TCWV fields has been attributed to the antenna to brightness temperature (Ta → Tb) conversion used by FNMOC (Ferraro, pers. comm.). If the Ta → Tb conversion of Wentz is used and the resulting brightness temperatures fed into the operational FNMOC TCWV algorithm, then the resulting TCWV product compares very well with the ASMU-A TCWV product.

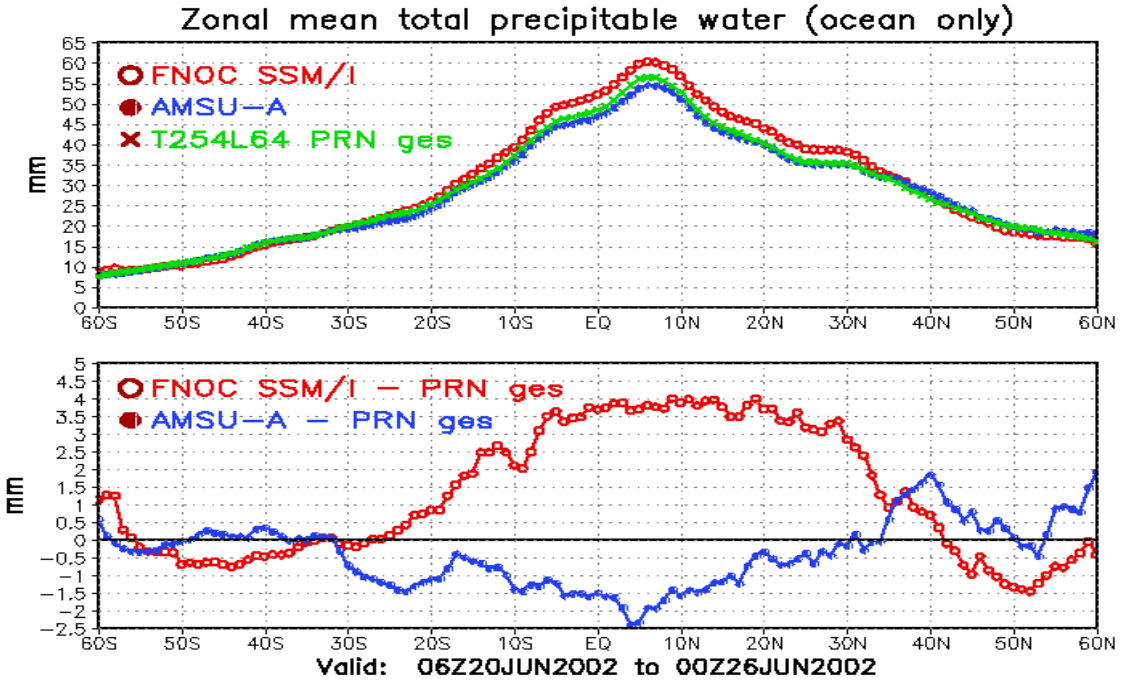

Figure 3 Zonal mean total column water vapor (upper panel), equivalently the total precipitable water, from SSM/I and AMSU-A algorithms along with values from T254L64 GFS background. Lower panel plots the difference between the microwave-derived products and the GFS background.

As a result of the discrepancy between SSM/I and AMSU-A TCWV products, assimilation of TCWV within the GDAS has been postponed. This experience with TCWV points to the need for a standard way to calibrate or, at least, document biases of similar products derived from various observational platforms. This experience again raises the issue of direct radiance assimilation. At the very least, direct radiance assimilation removes the added complexity of understanding the error characteristics of different retrieval algorithms.

4. Global Analysis

Both the global and regional analysis systems at NCEP utilize 3D-VAR to optimally combine available observations with a model-produced background. The EDAS also has a nudging component for the assimilation of precipitation (operationally) and cloud top pressure (experimentally). The GDAS has no nudging component.

The GDAS 3D-VAR (spectral statistical interpolation, SSI) has been running at NCEP since the early 1990s. Details regarding the SSI are found in Derber and Wu (1998) and references contained therein. Of interest here are aspects of the analysis pertaining to moisture.

The SSI analyzes spectral coefficients of specific humidity. Since the forward model for rain rates depends, in part, on cloud condensate, assimilation of rain rates forces a small increment in cloud condensate. Analyses of specific humidity and cloud condensate are univariate. Besides forcing from observations, a constraint term has been added to the objective function to penalize the analysis, x_a, for the generation of negative and supersaturated moisture values. The constraint term is

$$J_c(x_a) = \frac{1}{2}\sum_{i,j,k}\left\{\alpha_{i,j,k}\left(\frac{e_{i,j,k}(x_a)}{es_{i,j,k}(x_a)} < 0\right)^2 + \beta_{i,j,k}\left(\frac{e_{i,j,k}(x_a) - es_{i,j,k}(x_a)}{es_{i,j,k}(x_a)} > 0\right)^2\right\} \quad (3)$$

where, e is the vapor pressure and e_s is the saturation vapor pressure computed over a liquid water, mixed, or ice phase surface depending on the temperature. The constraint is effectively cast in terms of relative humidity and operates in grid space within the SSI inner minimization loop. The term is highly nonlinear and its introduction slows convergence of the minimization algorithm. The weights α and β have been set such that the number of negative and supersaturated points in the GFS background remains approximately unchanged following the analysis.

A version of the global 3D-VAR analysis that minimizes the objective function in grid-space has been developed by Wu *et al.* (2002). The grid space system (GSI) univariately analyzes pseudo-relative humidity (Dee and da Silva, 2002). At present, cloud condensate is not affected by the assimilation of precipitation. The GSI does not include a moisture constraint.

The analysis response to a single moisture observation in the absence of all other data and constraints is revealing. Relative humidity observations are placed at three locations as indicated in Table 1. Each analysis system is run once for each observation.

Location	Level	"Observed" RH (%)	Assumed observation error (%)	Guess RH (%)
60°E, 60°S	850 hPa	64.71	20	104.71
180°E, 0°	400 hPa	25.74	20	55.74
120°W, 30°N	700 hPa	65.84	20	15.84

Table 1 Location, level, value, and error of "observed" relative humidity along with the corresponding GFS background.

For the sake of brevity only the third case, a large positive perturbation with respect to the guess, is presented. Figure 4 plots a latitudinal cross section through the center of the analysis increment. A longitudinal cross section through 30°N reveals a similar structure. The vertical structure functions in the SSI yield a deeper response than those used in the GSI. Vertical correlations in the SSI are computed from

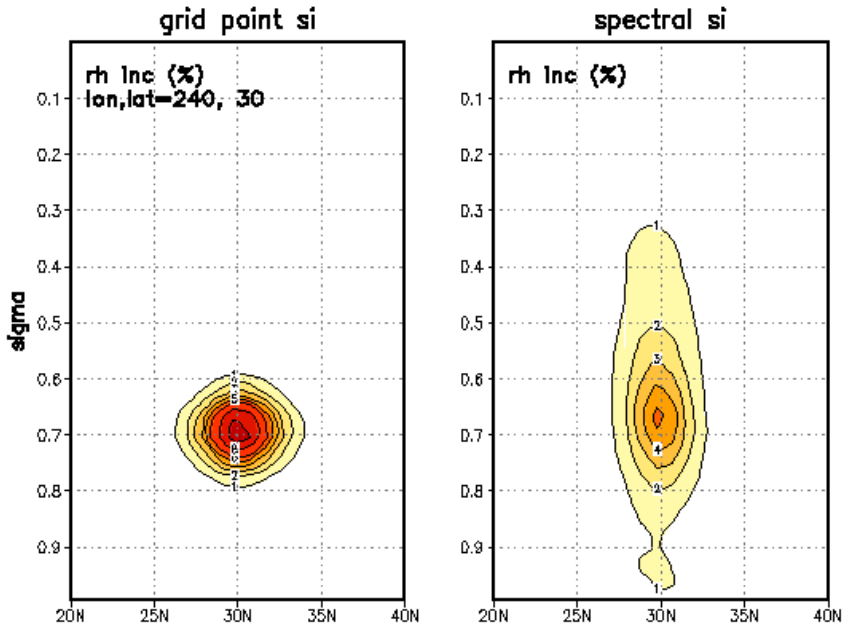

Figure 4 South-North cross section from 20°N to 40°N at 120°W of the relative humidity analysis increment from the GSI (left) and SSI (right). The contour interval is 1% relative humidity. The vertical coordinate is sigma, the GFS vertical coordinate.

an empirical orthogonal function decomposition of global vertical error covariance matrices for each analysis variable. In contrast, vertical scales in the GSI are locally estimated from statistics of the vertical correlation of each variable. The GSI increment is more in line with what would be expected given the small-scale nature of moisture.

Figure 5 shows the horizontal response, at the level of the observation, in both systems. A perturbation is seen in the SSI response not only at the observation location, but also at the mirror point on opposite side of the sphere (Fig. 5a). Transforms of a point perturbation between grid and spectral space partially explain this response. However, the formulation of the SSI error statistics also plays a role. SSI statistics are defined in wavenumber (i.e., global) space. Remote negative correlations can arise due to the truncation of these statistics at a finite wavenumber. Such remote correlations are unphysical and not desirable, especially for the moisture field, which by its very nature should have shorter correlation lengths.

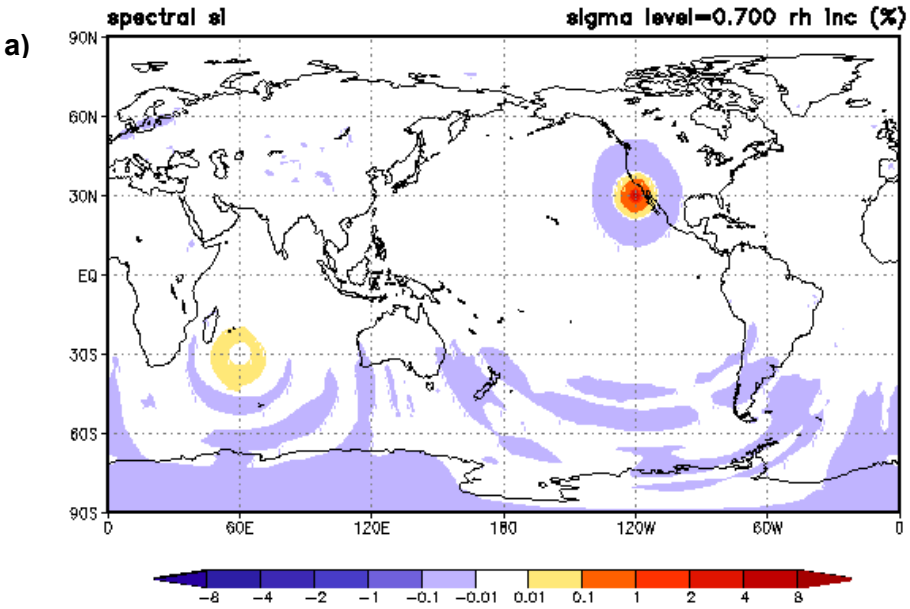

Fig. 5(a) SSI relative humidity analysis increment (%) at the observation level, σ=0.7.

The GSI error statistics, by design, do not possess such remote correlations. "Mirroring" effects are very weakly seen in the GSI response (Fig. 5b). This response arises from the grid to spectral transform at end of the GSI and then the inverse transform to create a gridded field for plotting. The localized response of the GSI intuitively appears more reasonable. An added benefit of the GSI, not yet fully developed, is the ability to accommodate inhomogeneous and anistotropic background error statistics. However, properly specifying the multiple degrees of freedom available in the GSI may prove increasingly problematic as higher resolutions are considered (Wu, *pers. comm.*). Still, the flexibility and initially encouraging GSI results argues for further evaluation.

As previously mentioned, the GDAS assimilates 1° superobs of SSM/I and TMI instantaneous rain rates. While the impact from each data set is minimal, much has been learned about the model physics and the impact of other observational data on GFS precipitation. A brief review of the assimilation of these precipitation observations within the GDAS follows.

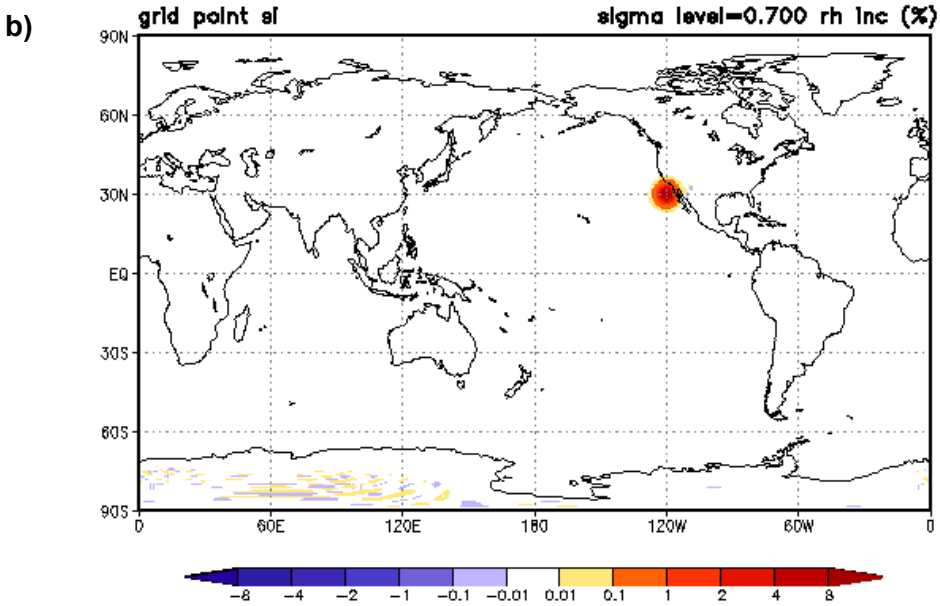

Fig. 5(b). GSI relative humidity analysis increment (%) at the observation level, s=0.7.

The forward model used to simulate rain rates is taking from the GFS moist physics. The model includes convective precipitation as parameterized by SAS and grid scale precipitation as described in Section 2. Total rain is the sum of convective and grid scale contributions using a fractional stepping approach. Input to the forward model consists of surface pressure, temperature, specific humidity, cloud condensate, zonal wind, and meridional wind. Of these, only surface pressure is not included as a control variable in the tangent linear (TLM) and adjoint models. As expected, simulated surface rain rates are most sensitive to the moisture and cloud condensate. Somewhat alarming, however, is the extreme sensitivity of surface rain rates to boundary layer temperature and water vapor (Fig. 6a).

As shown by Fillion and Mahfouf (2000), mass flux schemes, such as SAS, are extremely sensitive to the boundary layer temperature and moisture. The closure of these schemes effectively relies upon the calculation of convective available potential energy (CAPE) for a boundary layer parcel. The highly nonlinear nature of the CAPE calculation and its fundamental role in these schemes results in strong sensitivities. Schemes that do not depend upon CAPE in their closure, such as the Betts-Miller adjustment scheme, do not exhibit strong boundary layer sensitivities. The large boundary layer sensitivity of SAS significantly reduces the range of validity for the tangent linear model. This, in turn, leads to smaller step sizes and a slower rate of convergence in the SSI.

Ideally, one should, to the extent possible, modify the most nonlinear features of the precipitation physics to extend the range of validity for the TLM. Future updates to the forward model will address this point. For now, a more pragmatic approach has been taken. A smoothness check is added to the data pre-processing. Those observations for which the vertical derivative of the sensitivity profile exceeds a given tolerance are not assimilated. Figure 6b plots rainfall Jacobians for the same cases as in Fig. 6a, but following the smoothness check. The check flags about 5% of the SSM/I data and 4% of the TMI data.

The assimilated precipitation observation is actually the natural logarithm of the rain rate plus one. This formulation follows work done by Koizumi (2001) and Bauer et al. (2002) which suggests more tractable error specifications when dealing with a logarithmic transform. TMI observation errors were estimated by

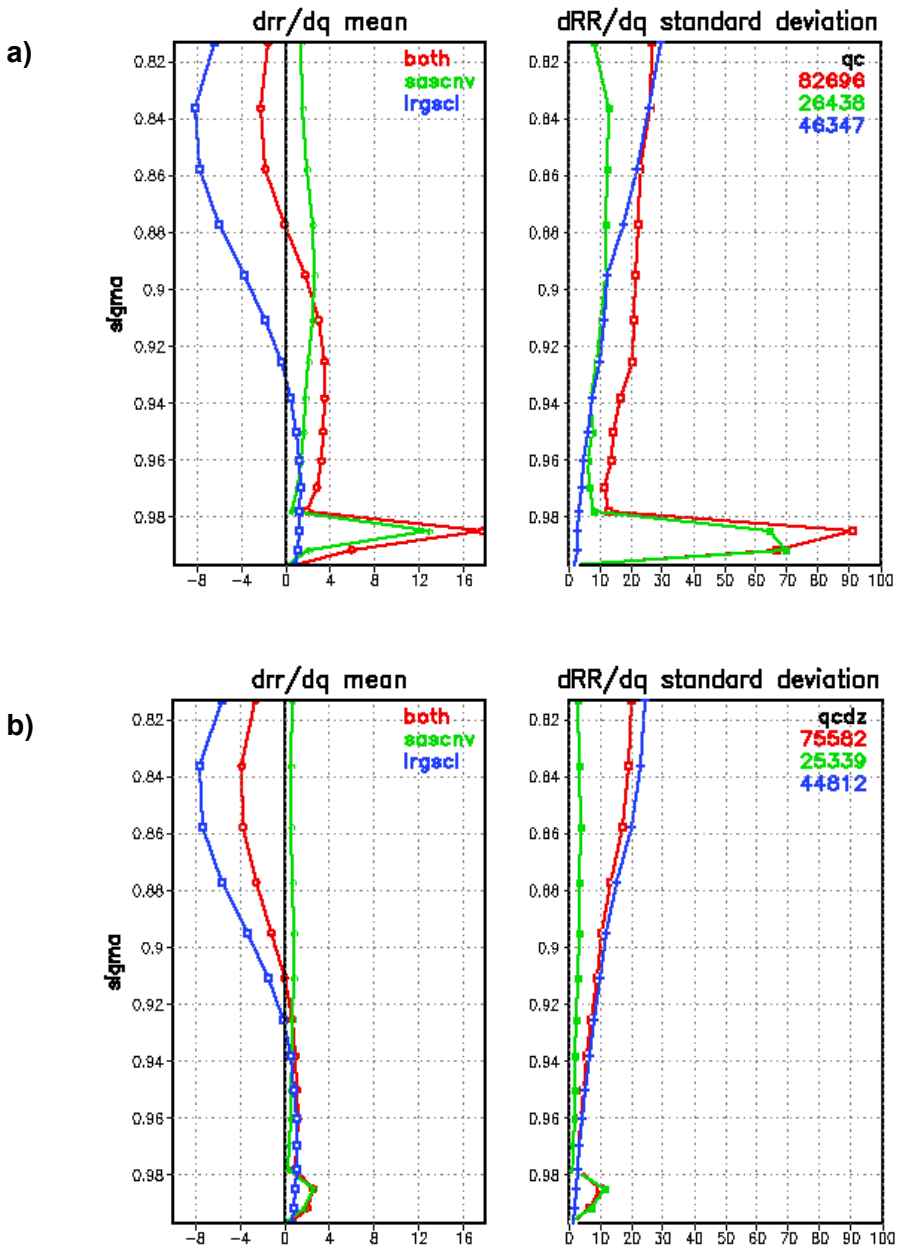

Figure 6 Mean (left panel) Jacobian of surface rain rate (mm h-1) to water vapor (g kg-1) perturbations. Vertical axis is the GFS vertical coordinate, s, from the surface to approximately 820 hPa. Jacobians are computed for convective only (green), grid-scale only (blue), and all (red) profiles. The standard deviation of the Jacobians is show on the right along with the number of profiles used in constructing each curve. (a) Profiles without sensitivity test. (b) following the sensitivity check.

comparing coincident TMI and TRMM precipitation radar rain rates for July 2001. A similar approach was taken for SSM/I rain rates with the ground "truth" being Stage III (see Section 5) rain rates over the continental United States for the period April-October 2001. Percent rain rate errors exceed 100% for rates less than 0.1 mm h-1. For this reason, rain rates below this threshold are not assimilated. However, zero rain rate (no rain) observations are used. Zero rain rates account for 89.4% and 78.7% of the total volume of SSM/I and TMI observations, respectively. The percentage observations falling in the (0.0,0.1) range is significantly smaller, 2.9% for SSM/I and 10.7% for TMI.

Given that rain rates can vary considerably over the 6 hour observational time window employed in the GDAS plus the fact that the SSI analysis is only valid for a given time (00, 06, 12 , or 18 UTC), time screening is applied to the observations. As the analysis relative time of the observation increases, the

quality control error bounds smoothly decrease to zero. The quality control bounds also decrease to zero for observations poleward of 45° latitude. Observations are not used over snow-covered land, ice covered water, and poleward of 60° latitude. These surface type and latitude checks screen out 15.6% of the SSM/I data (0.6% for TMI). Finally, those observations which deviate from the background rain rate by more than three times the estimated observation error are not assimilated. A limitation in the use of precipitation data not yet mentioned is the fact that the adjoint model provides no sensitivity information if the forward model is unable to simulate precipitation. The occurrence of nonzero observed rates with zero simulated rates is relatively small, 2.7% for SSM/I and 8.4% for TMI. However, given that only 7.7% of the SSM/I and 10.6% of the TMI observations have nonzero rain rates greater than 0.1 mm h-1, this fact significantly hampers the assimilation of higher observed rain rates. Nonlinear updates of the background during the outer loops and the influence of other data, especially radiance data, can initiate precipitation at initially non-precipitating points.

Out of the total volume of SSM/I and TMI observations, about 25% of the SSM/I and 14% of the TMI observations pass the smoothness check, time screen, and other quality control checks. This corresponds to approximately 7000 SSM/I and 1600 TMI observations per analysis cycle. The surface type and latitude checks are responsible for screening out the largest percentage of SSM/I observations. For TMI observations, it is the minimum rain detection test that screens out the largest percentage of potentially "useable" TMI data.

As an example of the impact of rain rate assimilation, a single case from the T254L64 GFS is presented. Compared with the SSM/I and TMI observations, the GFS precipitation is too widespread, especially in the extratropics (Fig. 7a). While 10.6% and 21.3% of the SSM/I and TMI observations have nonzero rain rates, these percentages increase to 48.9% and 28.6% for the GFS simulated rain rates. The greatest effect of rain rate assimilation is the reduction of this excessive precipitation (Fig. 7b). Increases in the simulated rain rates are more marginal.

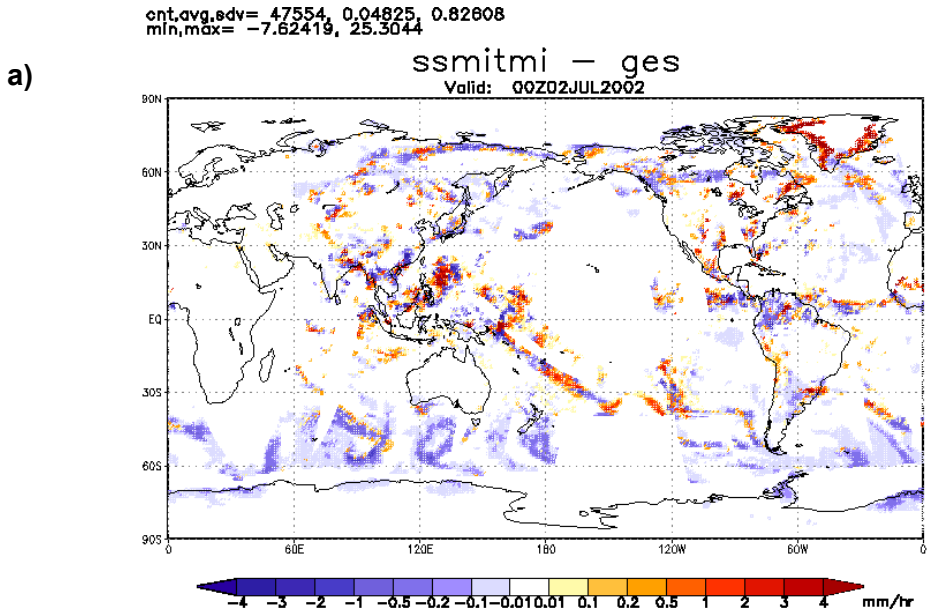

Figure 7 (a) SSM/I and TMI precipitation rates minus GFS forward model rates (mm h^{-1}), valid 00 UTC, 2 July 2002. The GFS background comes from the pre-implementation T254L64 GFS.

b)

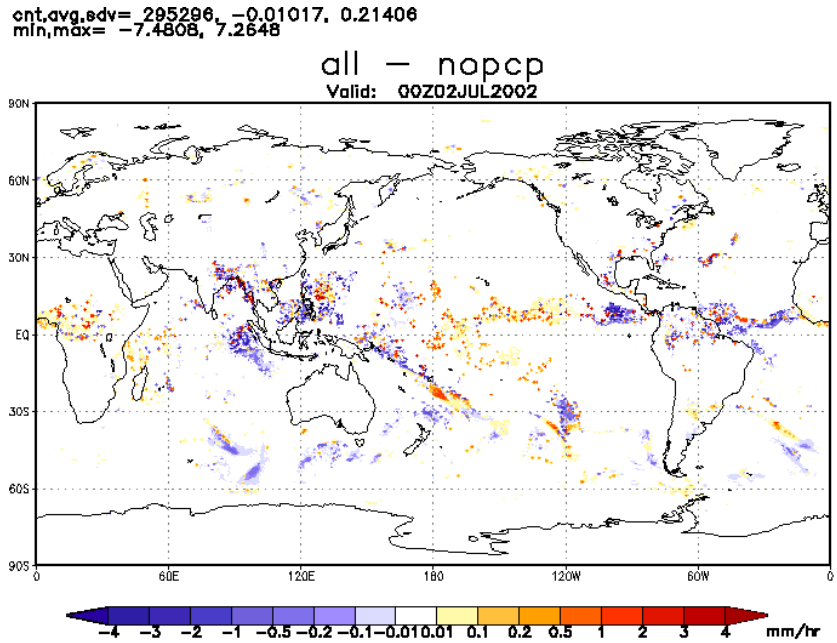

Figure 7(b) Same as (a) but following two analyses; one which assimilated SSM/I and TMI precipitation data ("all") and the other ("nopcp") which did not.

It is interesting to note that the assimilation of satellite radiances tends to increase model rain rates, especially in the tropics. Figure 8 illustrates this by plotting the difference between the single timestep precipitation for a GFS forecast initiated from a SSI analysis using all data, including SSM/I and TMI rain rates, and the background. Two factors are believed to be driving this response. First, the convective scheme used in the GFS is extremely sensitive to boundary layer moisture. While radiance observations have high horizontal resolution, their weighting functions span relatively deep vertical layers. Perhaps more importantly, the SSI vertical correlations are broad. Thus, moisture increments are spread over deep layers. Taken together these effects could easily generate the response seen in the simulated precipitation fields.

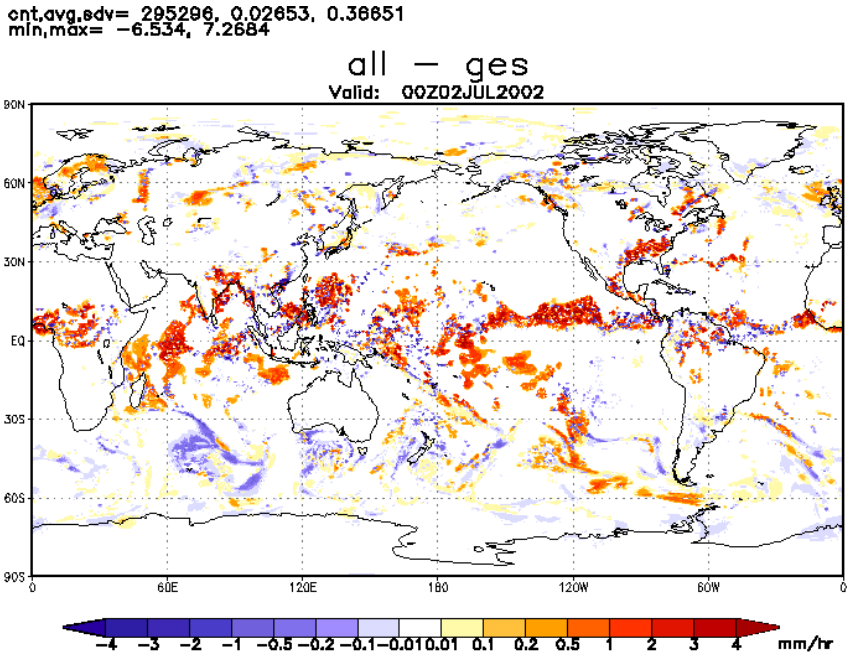

Figure 8 Difference in single timestep GFS rain rates (mm h-1), valid 00 UTC 2 July 2002.

5. Regional Analysis

The eta data assimilation system (EDAS) utilizes both precipitation and cloud top pressure observations in the analysis. Mention is made of both because (1) nudging, not a variational approach, is used to incorporate these data types, and (2) the EDAS cloud analysis is much more developed than that in the GDAS. Each EDAS analysis is preceded by a 12-hour pre-forecast analysis period. This period is broken into four three-hour forecast segments. 3D-VAR analyses connect the forecast segments. The 3D-VAR analysis uses the data mentioned in Section 3, while cloud top pressure and precipitation observations are assimilated via nudging during each three-hour forecast segment.

Details of the EDAS precipitation assimilation methodology are found in Lin *et al.* (2001). The assimilated precipitation observations come from the NCEP Stage II analysis (Baldwin and Mitchell, 1997; Seo, 1998). This product is based on automated hourly gauges and precipitation estimates from WSR-88D radars over the continental United States. At each time step and model grid point during the EDAS forecast for which a precipitation observation is available, the simulated and observed values are compared. Based on the difference, the model profiles of latent heat (temperature and specific humidity) and cloud water are adjusted so as to produce a precipitation amount consistent with the observed value. Benefits of precipitation assimilation include correcting the model's precipitation bias during the pre-forecast assimilation period, improving short-term precipitation forecasts, and providing superior forcing to the simulated soil moisture field.

Assimilation of GOES-8/10 cloud top pressure data is currently being evaluated in a parallel version of the EDAS. Nudging, again, is used to introduce the observations into the system. At each physics time step and each model grid column where observed cloud top is available, the model and observed cloud tops are compared. Above the observed cloud top, the model cloud water/ice is set to zero. At the same time, the water vapor mixing ratio is set to be no more than the appropriate (water or ice surface) saturated value. If the model air is sub-saturated at the observed cloud top, the model air is moistened over subsequent time steps such that the air will be saturated within one simulated hour. Finally, in the event that the precipitation assimilation requires the formation of a cloud, the observed cloud top is used to "anchor" the generated model cloud top. Preliminary results from this experiment show improvements in the innovations for rawinsonde winds, temperatures, and moisture along with increased equitable threat scores for precipitation forecasts.

6. Comments

This paper has briefly reviewed the analysis of moisture in the global and, to a lesser extent, the regional forecast/analysis systems run at NCEP. While progress has been made in the observation, analysis, and forecast of moisture, many issues remain open. What follows are comments, not necessarily conclusions, regarding some of these issues.

In terms of observations, the question of consistency between various products has become apparent as NCEP considers assimilating more hydrological parameters. For example, with respect to FNMOC SSM/I TCWV, GDAS analyses are dry in the tropics and moist in the extra-tropics. The differences are much smaller and, in fact, of the opposite sign (in terms of zonal means) when GDAS TCWV is compared with NESDIS Day-2 AMSU-A TCWV. The question, then, arises as to which product is closer to the "truth." Understanding and resolving the discrepancy between the SSM/I and AMSU-A products is a pre-requisite to using either for model verification or analysis purposes. A similar, though less surprising, difference is found when comparing AMSU-B rain rates (Day-2 algorithm) with those from SSM/I (FNMOC algorithm) and TRMM TMI (version 5). AMSU-B rain rates are considerably higher in the tropics. The TCWV and

rain rate examples point to the need for uniform standards when assessing the quality of various products. Estimates of similar parameters should be consistent. More realistically, differences between such products should be documented and, to the extent possible, accounted for.

The above comments point to the need for a better understanding of observation errors in general. Documenting and modeling the systematic and flow dependent components of these errors is necessary if data are to be used more effectively. Systematic error is likely to be a larger part of the total signal in moisture observations than other fields. The lack of high quality global validation data sets complicates efforts to quantify the error.

The issue of representativeness also arises when discussing errors. What does the "raw" observation actually measure? How strong is the link between the raw observable and the derived product? What relationship does the observable or product have to the analysis variables? What processes does the model actually resolve in contrast to those it parameterizes? Where in this spectrum does the observation fall?

With regards to satellite derived products the retrieval algorithms add another layer of complexity. Errors in the input radiances are convolved, usually nonlinearly, through the retrieval algorithms resulting in products with more complex error properties. For example, a preliminary study of ASMU-B rain rates errors suggests a significant scan angle component in the error (Kuligowski, *pers. comm.*). Modeling this error and bias correcting the data is non-trivial. For the purposes of data assimilation, the direct use of radiances may be preferable to retrieved products. Resources should be devoted to address and resolve the unique challenges of forward modeling of radiances in clear, cloudy, and precipitating fields of view. This effort takes on added significance in light of the rapidly growing volume of satellite data and the need to make the most consistent and complete usage of the data.

Utilizing radiances in cloud and precipitation regions requires more sophisticated forward models. In terms of forward models for moist physics, efforts need to be taken to minimize the impact of strong nonlinearities in these models. The valid range of the tanget linear models should equal that of typical analysis increments if the incremental variational approach is to be retained. Just as the bias and higher order error characteristics of observations need to be understood and modeled, the same must be done for forward models. Clearly these needs imply closer collaboration between those who develop forward models and those using these models in data assimilation.

The driving force behind any state of the art analysis schemes is proper specification of errors. Besides observation and forward model errors, errors in the background need to be understood and accurately represented. Before attempting to define the background error for moisture variable(s), a choice must be made as to the nature of the moisture variable(s). The SSI currently analyzes specific humidity. The grid point counterpart of the global analysis works with pseudo-relative humidity. This variable has the advantages of being more homogenous and covering a much smaller dynamic range than specific humidity. Future versions of the grid point system will have the additional advantage of being able to describe small scale, anisotropic, flow dependent features in the background error. However, both systems analyze moisture univariately. A question that requires further consideration is the possibility of building a moisture balance into the analysis. Temperature significantly affects moisture content and phase. Does a balance relationship of some sort lie within this relationship?

Even with improvements to observations, forward models, and analysis schemes, bias will likely remain an issue. Development of techniques which robustly and efficiently deal with model and data bias should not be ignored. A version of the SSI has been built to cycle not only the analysis but also the bias for analysis

variables. This system needs to be evaluated and developed further. Related to this is the need for enhanced monitoring of observations, analyses, and model forecasts. Reanalyses can serve a useful role in this effort.

References

Alihouse, J.C., S. Snyder, J. Vongsathorn, and R.R. Ferraro, 1990: Determination of oceanic total precipitable water from the SSM/I. *IEEE Trans. Geo. Rem. Sens*., **28**, 811-816.

Baldwin, M. E., and K.E. Mitchell, 1997: The NCEP hourly multi-sensor U.S. precipitation analysis for operations and GCIP research. *Preprints, 13th AMS Conference on Hydrology*, Long Beach, CA, 54-55.

Bauer, P, J.-F. Mahfouf, W.S. Olson, F.S. Marzano, S.D. Michele, A. Tassa, and A. Mugnai, 2002: Error analysis of TMI rainfall estimates over ocean for variational data assimilation. *Quart. J. Roy. Meteor. Soc.*, in press.

Chou, M.D., M. J. Suarez, C. H. Ho, M. M. H. Yan, and K. T. Lee, 1998: Parameterizations for cloud overlapping and shortwave single scattering properties for use in general circulation and cloud ensemble models. *J. Climate*, **11**, 202-214.

Colton, M.C., and G.A. Poe, 1994: Shared processing program, defense meteorological satellite program, special sensor microwave/imager algorithm symposium, 8-10 June 1993., *Bull. Amer. Meteor.* Soc., **75**, 1663-1669.

Dee, D. P., and A. M. da Silva, 2002: On the choice of variable for atmospheric moisture analysis. To appear in *Mon. Wea. Rev.*

Derber, J.C., and W.-S Wu, 1998: The use of TOVS cloud-cleared radiances in the NCEP SSI analysis system. *Mon. Wea. Rev.*, **126**, 2287-2299.

Ferraro, R.R., 1997: SSM/I derived global rainfall estimates for climatological applications. *J. Geophy. Res.,* **102**, 16715-16735.

Fillion, L., and J.-F. Mahfouf, 2000: Coupling of moist-convective and stratiform precipitation processes for variational data assimilation. *Mon. Wea. Rev.*, **128**, 109-124.

Grody, N., J. Zhao, R.R. Ferraro, F. Weng, and R. Boers, 2001: Determination of precipitable water and cloud liquid water over ocean from the NOAA-15 advanced microwave sounding unit. *J. Geophy. Res*., **106**, 2943-2953.

Heymsfield, A. J., and G. M. McFarquhar, 1996: High albedos of cirrus in the tropical Pacific warm pool: microphysical interpretations from CEPEX and from Kwajalein, Marshall islands. *J. Atmos. Sci*., **53**, 2424-2451.

Kiehl, J.T., J. J. Hack, G. B. Bonan, B. A. Boville, D. L. Williamson, and P. J. Rasch, 1998: The national center for atmospheric research community climate model CCM3. *J. Climate*, **11**,1131-1149.

Koizumi, K., 2001: The four-dimensional variational data assimilation system for the JMA mesoscale model. *Preprints, 14th AMS Conference on Numerical Weather Prediction*, Fort Lauderdale, FL. J96-J98.

Kummerow, C.D., Y. Hong, W.S. Olson, S. Yang, R.F. Adler, J. McCollum, R.R. Ferraro, G.W. Petty, D.-B. Shin, and T.T. Wilheit, 2001: The evolution of the Goddard Profiling Algorithm (GPROF) for rainfall estimation from passive microwave sensors. *J. Appl. Meteor.*, **40**, 1801-1820.

Lin, Y., M. E. Baldwin, K. E. Mitchell, E. Rogers, and G. J. DiMego, 2001: Spring 2001 changes to NCEP Eta analysis and forecast system: assimilation of observed precipitation data. *Preprints, 14th AMS Conference on Numerical Weather Prediction*, Fort Lauderdale, FL. J92-J95.

Seo, D.J., 1998: Real-time estimation of rainfall fields using radar rainfall and rain gauge data. *J. Hydro.*, **208**, 37-52.

Slingo, A., 1989: A GCM parameterization for the shortwave radiative properties of water clouds. *J. Atmos. Sci.*, **46**, 1419-1427.

Stephens, G. L., 1984: The parameterization of radiation for numerical weather prediction and climate models. *Mon.Wea. Rev.*, **112**, 826-867.

Sundqvist, H., E. Berge, and J. E. Kristjansson, 1989: Condensation and cloud studies with mesoscale numerical weather prediction model. *Mon. Wea. Rev.*, **117**, 1641- 1757.

Weng, F. and N. Grody, 2000: Retrieval of ice cloud parameters using a microwave imaging radiometer. *J. Atmos. Sci*., **57**, 1069-1081.

Wu, W.-S., R. J. Purser, and D. F. Parrish, 2002: Three dimensional variational analysis with spatially inhomogeneous covariances. To appear in *Mon. Wea. Rev.*

Xu, K. M., and D. A. Randall, 1996: A semiempirical cloudiness parameterization for use in climate models. *J. Atmos. Sci.*, **53**, 3084-3102.

Zhao, L. and F. Weng, 2002: Retrieval of ice cloud parameters using the Advanced Microwave Sounding Unit (AMSU). *J. Appl. Meteor.* **41,** 384-395.

Zhao, Q. Y., and F. H. Carr, 1997: A prognostic cloud scheme for operational NWP models. *Mon. Wea. Rev.*, **125**,1931- 1953.